

Co-evolution of nodes and links: diversity driven coexistence in cyclic competition of three species

Kevin E. Bassler*

*Department of Physics, Department of Physics, University of Houston, Houston, TX 77204-5005, USA
Texas Center for Superconductivity, University of Houston, Houston, TX 77204-5002, USA and
Max-Planck-Institut für Physik komplexer Systeme,
Nöthnitzer Str. 38, Dresden D-01187, Germany*

Erwin Frey†

*Arnold Sommerfeld Center for Theoretical Physics and Center for Nanoscience, Department of Physics,
Ludwig-Maximilians-Universität München, Theresienstrasse 37, 80333 München, Germany*

R. K. P. Zia‡

*Max-Planck-Institut für Physik komplexer Systeme,
Nöthnitzer Str. 38, Dresden D-01187, Germany and
Center for Soft Matter and Biological Physics, Department of Physics,
Virginia Polytechnic Institute and State University, Blacksburg, VA 24061, USA*

(Dated: August 20, 2018)

When three species compete cyclically in a well-mixed, stochastic system of N individuals, extinction is known to typically occur at times scaling as the system size N . This happens, for example, in rock-paper-scissors games or conserved Lotka-Volterra models in which every pair of individuals can interact on a complete graph. Here we show that if the competing individuals also have a “social temperament” to be either introverted or extroverted, leading them to cut or add links respectively, then long-living state in which all species coexist can occur when both introverts and extroverts are present. These states are non-equilibrium quasi-steady states, maintained by a subtle balance between species competition and network dynamics. Remarkably, much of the phenomena is embodied in a mean-field description. However, an *intuitive* understanding of why diversity stabilizes the co-evolving node and link dynamics remains an open issue.

I. INTRODUCTION

Evolutionary game theory [1, 2] considers populations composed of individuals with different strategies or behavioral programs who compete generation after generation in game situations of the same type. A central question is how evolutionary forces like natural selection and mutation shape the time evolution of a population. In particular, one is interested to learn about mechanisms underlying maintenance of species diversity and extinction of species. Typically one studies fixed environments which may be, for example, well-mixed or spatially extended systems, where the players of the game are located at the nodes of a complete graph or a regular lattice, respectively. On another front, much of network science [3–5] has been devoted to the study of the structure or topology of the links in a graph, while the nodes have no degrees of freedom. Though the properties of static networks, such as Erdős-Rényi random graphs [6], have received considerable attention, there has also been interest in networks with links that evolve dynamically, such as in the formation of scale-free networks by preferential attachment [7, 8]. Bringing together these two

paradigms, statistical mechanics of node degrees of freedom connected by fixed links and networks with an evolving link topology, is the central motivation of our work. Clearly, in many complex systems in nature, the evolution of both components must be accounted for simultaneously.

Studies of networks that have ‘co-evolving’ nodes and links, also known as ‘adaptive networks’, began to emerge about two decades ago [9–13]. In attempts to model realistic co-evolving systems, complex mathematical structures and serious challenges are encountered. In this context, we introduce a minimal system of node and link degrees of freedom, co-evolving with stochastic rules. Finding unexpected, novel behavior in extensive numerical simulations, we exploit the simplicity of the model to derive tractable mean-field equations and to obtain some analytic results. This study should be regarded as one of a few first steps towards investigating more complex and realistic co-evolving systems.

Our model combines the node dynamics of the well known rock-paper-scissors game [2, 14], also known as cyclic Lotka-Volterra model [15–17], and the link dynamics in recent studies of networks with preferred degrees [18–23]. In the former, the three ‘species’ compete cyclically and, if N individuals play stochastically on a complete network, and the typical extinction time scales with the population size N [24]. In the latter system, designed to model the actions of individuals with differ-

* bassler@uh.edu

† frey@lmu.de

‡ rkpzia@vt.edu

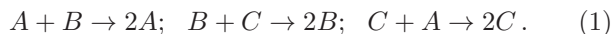
ent ‘social temperaments’ – introverts and extroverts – are considered. The links fluctuate as a randomly chosen individual cuts or adds connections. Even in a simple population with extreme temperaments, surprising behavior emerged [20, 22, 23]. Here, we consider a system with nodes that can be one of three species and can have one of two temperaments, with specific rules of evolution for both the nodes and links. When a link between two nodes is absent, they do not interact, so that the competition between the three species is both ‘tempered’ and dynamic. In a following, we report simulation results with N up to 1000, as well as a theoretic description, based on mean-field approximation. Specifically, we discover long-living, *quasi-stationary states* (QSS), persisting for up to $O(10^{12})$ node changes. For these QSS to occur, nodes with both temperaments must be present. Thus, we refer to this kind stability as ‘diversity driven coexistence.’

In the next section, we specify the setup of our model and its dynamics. Results from simulation studies and analysis of a set of mean-field equations are presented in a following section. It is natural that findings of the QSS states raise more interesting questions for future research. These issues, as well as an outlook for exploring more realistic models of co-evolution, are discussed in the final section.

II. SPECIFICATIONS OF THE MODEL

Our model of co-evolution consists of merging two of the simplest statistical systems, each involving node or link dynamics only. The former is designed for neutral cyclic competition amongst three species. Known as the cyclic Lotka-Volterra model, it is often portrayed as the game of rock-paper-scissors. Here we refer to it here as the *ABC* model [16, 24]. The latter consists of a network of links, cut or added by a collection of ‘introverts’ (I) and ‘extroverts’ (E), the extreme case of which is the *XIE* model [19, 20]. Thus, we will refer to the union as the *ABC-XIE* model.

For the *ABC* component, let us follow the notation of Refs. [24, 25] and consider the simplest possible scenario: a system with N individuals, each being one of three ‘species’ (A, B, C), competing cyclically with unit rates:



With no spatial structure, the configuration of a ‘well-mixed’ system is completely specified by the numbers of each ($N_{A,B,C}$) with the total number $N = N_A + N_B + N_C$ being a constant of motion. In the large N limit, the evolution is well approximated by a deterministic set of ‘chemical rate’ equations:

$$\partial_t N_A = N_A N_B - N_C N_A \quad \text{and cyclic,} \quad (2)$$

where t is appropriately normalized (all rates are taken as unity). It is well-known that $R \equiv N_A N_B N_C$ is a

constant of motion of these equations, so that the orbits in configuration space form closed loops and extinction never occurs [14]. In this sense, the competition is ‘neutral’. However, if stochastic aspects of the evolution is included, then extinction of two of the species is inevitable for finite systems, typically in $O(N)$ steps [15, 24]. Indeed, highly counter-intuitive behavior is found when the competition rates are unequal [25]. Similarly, many interesting phenomena emerge when such systems are placed into some spatial structure [26–34], in which an individual may interact with, say, only nearest neighbors in a lattice.

For the *XIE* component, the simplest version [19, 20, 22] consists of a fixed number of introverts and extroverts, connected by a network with dynamic links that change as a result of the action of a randomly chosen individual: An I will cut one of its existing links while an E will add a link to an individual it is not already connected to. With random sequential update, this simple model displays an extreme Thouless effect: an extraordinary transition when the numbers of the subgroups are equal [22].

Our interest here is to study the importance of behavioral diversity in games of cyclic dominance. To do so we merge the *ABC* and *XIE* models, by endowing the individuals of the *ABC* model with a temperament, $\tau \in \{I, E\}$. To avoid confusion, we will denote ‘species’ by $\alpha \in \{A, B, C\}$, so that an individual’s state is given by (α, τ) . In this sense, each node can be one of six ‘types’: $A_{I,E}$, $B_{I,E}$, and $C_{I,E}$. A system configuration is specified by $\mathcal{C}: \{(\alpha, \tau)_i; a_{ij}\}$, where $i, j \in \{1, \dots, N\}$ label an individual and a_{ij} are elements of \mathbb{A} , the adjacency matrix describing the presence or absence of links. Thus, $a_{ij} = 1/0$ if the link between i and j is present/absent. There are no self-loops: $a_{ii} \equiv 0$.

A related model has studied cyclic dominance on an adaptive network in a model of opinion spreading [35]. However, the link dynamics were very different in that model. All nodes behaved identically. Link updates were coupled to the outcome of node interactions through an *ABC* competition. A losing node either chose to adopt the ‘opinion’ of the winner, indicated by its *ABC* state, or cut its link with the winner and rewired that link by connecting it to another, randomly selected, node. All nodes therefore maintained their initial degree. Depending on the density of links and the propensity of losing nodes to rewire versus changing their opinion, a variety of behavior can occur, including both reaching consensus and network fragmentation.

In our model the system evolves according to the following rules: From any configuration \mathcal{C} , in a Monte Carlo sweep (MCS), we execute N updates, each of which consists of choosing a random pair of nodes and, with probability r and $(1-r)$, attempt to change the states of, respectively, nodes and links. Suppose the pair (i, j) is chosen. For a node-update, if $a_{ij} = 0$ or if $\alpha_i = \alpha_j$, then \mathcal{C} remains unchanged, but a pair with a link connecting it ($a_{ij} = 1$) and $\alpha_i \neq \alpha_j$ (regardless of $\tau_{i,j}$) will

be changed according to the rules (1), while all links are *unaffected*. Additionally, the temperament of the winning node in the *ABC* cyclic competition is inherited by the ‘offspring’. For example, when an *AC* pair turns into *CC*, both of the nodes at the end have the temperament that the original *C* node had. On the other hand, for a link-update, the nodes remain *unchanged*, while the link value a_{ij} is *assigned*, regardless of its previous state, to be 1 or 0 if the temperaments $(\tau_{i,j})$ are both *E*’s or both *I*’s, respectively. If $\tau_i \neq \tau_j$, a_{ij} is set to 1 or 0 with equal probability. This link update rule is not the one introduced in the original *XIE* model [20]. Instead, it is in the spirit of ‘heat-bath dynamics’ that often are used in simulations of the Ising model [36–38]. Though such a rule does not lead to the remarkable behavior reported in [20, 22], it does allow tractable differential equations for the link dynamics to be written. Such a simplification is justifiable, as this study is an exploration of systems with node-link co-evolution.

The full stochastic dynamics can – given the above rules – be written in terms of a master equation for the probability to observe a system configuration \mathcal{C} at time t , $P(\mathcal{C}, t)$, and solved exactly employing a stochastic Gillespie simulation [39]; see next section. Here, we briefly discuss some general features of the stochastic dynamics. First, one should note that if the population of one of the node types ever vanishes, then it will remain zero: there is no mechanism to create a species anew. Let’s consider some limiting cases first:

1. $r = 0$: There is no node dynamics. With frozen nodes states, the system reverts simply to the *XIE*-model with fixed number of *I*’s and *E*’s. Only the *I-E* links fluctuate between being present and absent. The steady state probability distribution $P^*(\mathbb{A})$ is a simple product of appropriate $p(a_{ij})$ ’s.
2. $r = 1$: There is no link dynamics. The network is frozen at the initial topology, on which the final state crucially depends, as the system evolves with only the *ABC*-dynamics. Depending on the topology of the network interesting phenomena emerge [40–42].
3. If the *I*’s go extinct and $r \neq 0, 1$, then the network will quickly evolve to a complete graph and the system reverts to the well-mixed *ABC*-model.
4. If instead, the *E*’s go extinct, then all links will eventually disappear and any $\{\alpha_i\}$ is an absorbing state.
5. If any $\alpha \in \{A, B, C\}$ goes extinct, the competition among the remaining two is trivial, though the final state may again consist of arbitrary ratios provided they are all introverts (where all links are absent).

From these limits, one aspect is clear: there are many absorbing states for $r > 0$. Here we are not interested in

calculating extinction times but in identifying and characterizing non-trivial, long-living, ‘quasi-stationary’ states (QSS), similar as the ‘active states’ in many epidemic models.

There are only two control parameters, N and r , in our model. By contrast, there are many ‘order parameters,’ characterizing the collective behavior of this system. The most natural set consists of $27 = 6 + 21$ quantities: $N_{\alpha,\tau}$, the total number of each node type, as well as $L_{\alpha,\tau;\alpha',\tau'}$, the total number of existing links between individuals of each pair of types. Of course, the set of N ’s is constrained by $N = \sum_{\alpha,\tau} N_{\alpha,\tau}$. At any given time, not every individual of type (α,τ) is connected to every one of type (α',τ') . Therefore $L_{\alpha,\tau;\alpha',\tau'}$ is a fluctuating quantity, even for configurations with fixed $N_{\alpha,\tau}$ and $N_{\alpha',\tau'}$. Also, unlike the absence of self-loops ($a_{ii} \equiv 0$), the links between individuals of a single type ($L_{\alpha,\tau;\alpha,\tau}$) is a non-trivial, dynamic variable (lying in the range $[0, N_{\alpha,\tau}(N_{\alpha,\tau} - 1)/2]$).

III. STOCHASTIC SIMULATIONS AND MEAN-FIELD THEORY

Using Monte Carlo simulations, our initial explorations began with a random collection of all six nodes types, with N up to 1000, connected by a random, half filled network. Not surprisingly, the early stages of the dynamics appear ‘chaotic’ with 27 intertwined variables. Often, extinction of species sets in quite quickly. However, in many of the simulation runs, the system settles into relatively regular and long-living QSS. We find that these QSS contain the ‘most diverse’ set of three node types, namely, all three species and both temperaments are present. Of course, we may expect this behavior, given our discussion above on the limiting cases (3-5). Since they appear to be more tractable, we will devote our attention only to such QSS in the rest of this paper.’

There are two distinct classes of ‘diverse’ QSS. Exploiting cyclic symmetry, they can be labeled as $A_E B_E C_I$ or $A_E B_I C_I$. For simplicity, we will focus here mainly on the former and only comment briefly on the latter. In either cases, α and τ are uniquely related and, from now on, we will drop the τ label and write, e.g., N_A and L_{BC} instead of N_{A_E} and $L_{B_E C_I}$, respectively. To re-emphasize, our *A*’s and *B*’s are extroverts, while *C*’s are introverts.

Of course, the links in our system are non-directional, so that $L_{\alpha\beta} = L_{\beta\alpha}$. Thus, there are only 3 N ’s and 6 L ’s to monitor, numbers that can be regarded as particles in 3 ‘square boxes’ and 6 ‘round urns’; see Fig. 1. Furthermore, the 3 N ’s are constrained: $N = \sum_{\alpha} N_{\alpha}$, leaving 8 independent numbers. When a node changes its state, say through an $A + B \rightarrow 2A$ update, a particle moves from one box to another (denoted by the thin arrows in Fig. 1). All the links to this node will also change character, and the corresponding particles in the urns must move also (denoted by the thick arrows in Fig. 1). These considerations will play a key role when we derive approx-

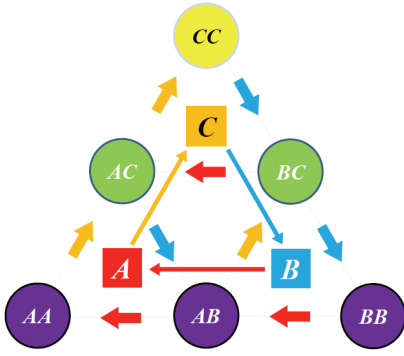


FIG. 1. Schematic diagram showing the results of a node update in a $A_E B_E C_I$ QSS, showing the co-evolutionary nature of the dynamics. Particles in the square boxes represent individuals of each node type, while those in circular urns represent links of the appropriate category. The dark urns (purple-online) represent E-E links. While the medium (green-online) and light colored (yellow-online) urns represent I-E and I-I links, respectively. If a node changes in, say, an $A+B \rightarrow 2A$ update, then a particle moves from box B to box A , represented by the long thin dark gray (red-online) arrow. All the links that the changed node has also change, thus particles moves from urns BA , BB , and BC to urns AA , AB , and AC , respectively, represented by the short thick dark gray (red-online) arrows. The medium gray (blue-online) and light gray (yellow-online) arrows indicate the particle moves resulting from $B+C \rightarrow 2B$ and $C+A \rightarrow 2C$ updates, respectively. By contrast, during a link update, at most, a single particle will be added to or removed from the appropriate urn.

imate mean-field equations for $\partial_t L_{\alpha\beta}$. By contrast, the moves associated with a link update are simple: adding or removing a ‘particle’ in an urn. For example, if an unconnected AB pair is chosen, then we would add a ‘particle’ to the L_{AB} urn (always, in this case). Note that the urns on each row are updated with the same rule: Always remove one at the top (CC), always add for urns at the bottom row, and add/remove with equal probability for those in the middle.

To focus on the QSS in simulation studies, various values of (N, r) were chosen. The system was typically initialized near the symmetry point ($N_\alpha \cong N/3$) and randomly half-filled with links. It was then evolved for up to $\sim 10^9$ MCS, during which time the 9 variables were measured. We first discovered that, for a narrow range of r , the life time of a QSS can be orders of magnitude longer than the typical extinction time of the ABC model, as much as $O(10^5)$ MCS. Encouraged by the presence of such unexpected longevity, and seeking insight into the QSS’s, we postulated a set of equations for the evolution of the macroscopic quantities, based on a mean-field approach and discussed below. The fixed points and their associated stability properties led us to perform further simulations at $r \cong 4/N$. At this value of r , runs with $N = 1000$ remain active after 10^9 MCS! Figure 2 illustrates the typical behavior in such a QSS, more details

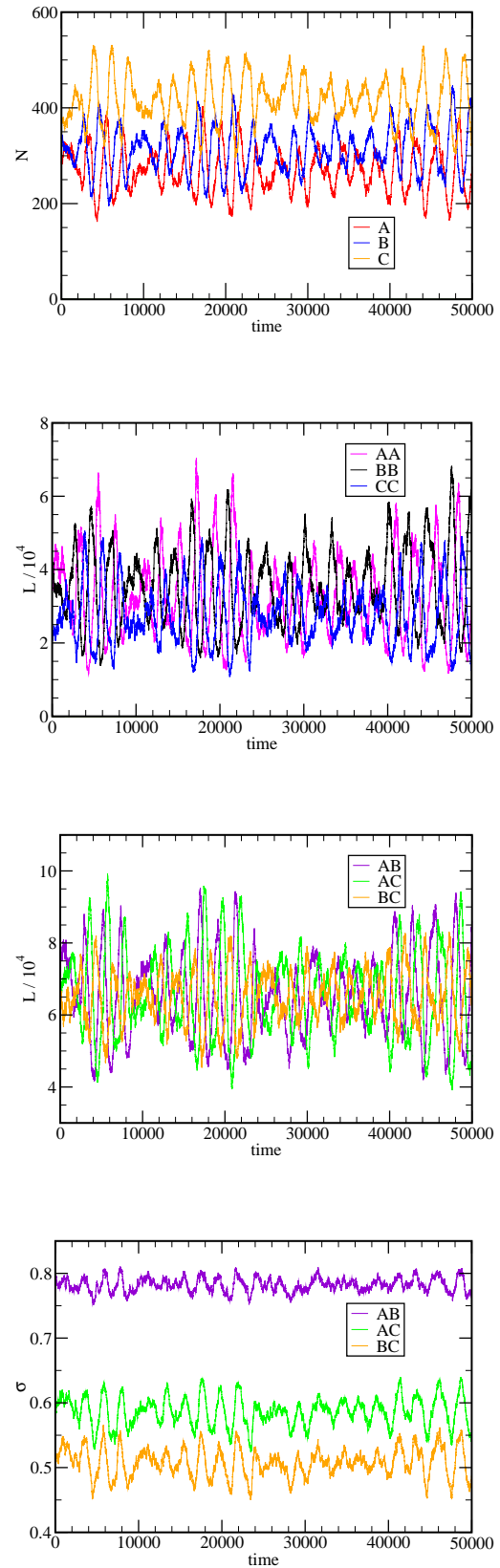


FIG. 2. Results from a very long (10^9 MCS) run with $N = 1000$ and $r = 4/N$. Figures show a typical 5×10^4 section of, from top to bottom, a) population numbers of A , B , and C . b) total self-links AA , BB , and CC . c) total cross-links AB , AC , and BC . d) fraction of cross-links, which are remarkably in phase.

of which will be discussed below.

Let us first consider the mean-field equations, however, as they provide some insight into the nature of the co-evolving system. The full equations are given in the Appendix. Here we only outline their derivation. Formulating how the node variables change is straightforward. They only change through node updates, which occur with rate r , and during which a chosen link, if present, will lead to one of its nodes being altered. For example, there are L_{AC} links connecting an A and a C . If one of these links is chosen and a node update is attempted, then N_A will decrease by one and N_C will increase by one. Thus, instead of Eq. (2), we may write

$$\partial_t N_A = r(L_{AB} - L_{AC}) \quad \text{and cyclic.} \quad (3)$$

Unlike the standard ABC -model, the action of the I 's means that $L_{\alpha\beta} < N_\alpha N_\beta$ typically. Thus, we define a useful variable,

$$\sigma_{\alpha\beta} \equiv L_{\alpha\beta}/N_\alpha N_\beta, \quad (4)$$

which plays the role of an effective interaction rate in Eq. (1). For example, we can cast the $\partial_t N_A$ equation above as $\partial_t N_A = r\sigma_{AB}N_A N_B - r\sigma_{AC}N_A N_C$. Though this form is neater, the presence of the variables σ signals complications, as the derivation of the link equations below will show. Note that, since the nodes do not change during link-updates, there are no terms proportional to $(1-r)$. Of course, the equations for the different node variables sum to $\partial_t N = 0$ as N is a constant of motion.

Describing the evolution of the link variables $L_{\alpha\beta}$ is more involved, as it is affected by both kinds of updates. There are terms due to link updates, which occur at a rate of $(1-r)$: a chosen link will be cut or added according to the temperament of its two nodes, and the number of I - I (E - E) links can only decrease to zero (increase towards the maximal value), while the I - E links are driven towards half of the maximum value. Thus, we have $(r-1)L_{CC}$ in the $\partial_t L_{CC}$ equation, and e.g., $(r-1)\{L_{AC} - N_A N_C/2\}$ in the $\partial_t L_{AC}$ equation, and $(r-1)\{L_{AB} - N_A N_B\}$ in the $\partial_t L_{AB}$ equation. In addition, terms proportional to r are needed to account for changes induced by a node-update, as shown by the thick arrows in Fig. 1. At the microscopic level these terms involve the probability of 3-node (say, A , B , and γ) clusters. Consider choosing a *particular* connected AB pair, which will change to an AA pair, under our rules. But then, all the *other* links this B had will also change, as a $B\gamma$ link is now an $A\gamma$ link, and the 3-node cluster changes: $A-B-\gamma \rightarrow A-A-\gamma$. Denoting the number of γ 's linked to B by $k_{B\gamma}$, we see that $L_{A\gamma}/L_{B\gamma}$ gains/loses by this amount. Unfortunately, a complication is that $k_{B\gamma}$ differs from one B node to another. In the spirit of mean-field theory, we replace it by the average, namely, $L_{B\gamma}/N_B$. Such standard approximation schemes for moment closure [35] can be exploited to arrive at a set of terms for the link equations. For example, in the $\partial_t L_{AB}$ equation, we would include gain

terms like $L_{BC}k_{CA} \simeq L_{BC}L_{CA}/N_C$ (from choosing the BC pair in a cluster linked as B - C - A) and loss terms like $-L_{CA}k_{AB} \sim -L_{AC}L_{AB}/N_A$ (from choosing the CA pair in a cluster linked as C - A - B). The result of such straightforward but tedious considerations are given as the first set of equations in the Appendix. Together with the set of Eq. (3), these will be the basis of our theory.

To continue, it is convenient to define the fractions

$$\eta_\alpha \equiv N_\alpha/N, \quad (5a)$$

$$\lambda_{\alpha\beta} \equiv 2L_{\alpha\beta}/N(N-1), \quad (5b)$$

and consider the ‘thermodynamic limit’: $N \rightarrow \infty$ with

$$\rho \equiv r(N-1)/2 \quad (6)$$

fixed. Then rescaling t by N , only one control parameter, ρ , remains [43]. The full set of mean-field equations for these variables simplify slightly, as shown in the Appendix. We provide two examples here:

$$\partial_t \eta_A = \rho(\lambda_{AB} - \lambda_{CA}), \quad (7)$$

$$\begin{aligned} \partial_t \lambda_{AB} = \rho \left\{ \frac{\lambda_{BC}\lambda_{CA}}{\eta_C} - \frac{\lambda_{AB}\lambda_{AC}}{\eta_A} + 2\frac{\lambda_{BB}\lambda_{BA}}{\eta_B} - \frac{\lambda_{AB}^2}{\eta_B} \right\} \\ - \{\lambda_{AB} - 2\eta_A\eta_B\}. \end{aligned} \quad (8)$$

Despite these simplifications, it is not feasible to solve these equations analytically. Even the fixed point equations involve solving non-linear (algebraic) equations for 5 variables. Before discussing the numerical results, let us offer some insight into their behavior.

First, note that the fraction of the total number of links, $\lambda \equiv \sum_\alpha \lambda_{\alpha\alpha} + \sum_{\alpha \neq \beta} \lambda_{\alpha\beta}$, satisfies a very simple equation:

$$\partial_t \lambda = (1-r)\{\eta_A + \eta_B - \lambda\} \quad (9)$$

Here we keep $(1-r)$, instead of writing $(1-2\rho/N) \rightarrow 1$, to highlight the absence of r terms in the evolution of the total link-number, which is conserved during node-updates. Equation (9) is intuitively reasonable, as it simply forces λ to follow the fraction of extroverts.

As a next step we study the fixed points of the mean-field equations (denoted by a superscript: $*$) and their neighborhoods. Despite some simplifications ($\lambda_{AB}^* = \lambda_{BC}^* = \lambda_{CA}^* \equiv x^*$, $\lambda^* = \eta_A^* + \eta_B^*$), the analytic form of $(\eta_\alpha^*, \lambda_{\alpha\beta}^*)$ is quite complex (as they are solutions of non-linear equations for 5 variables). Let us discuss briefly the simpler $r \rightarrow 0, 1$ limits. For the former ($r \rightarrow 0$), the rapid link dynamics leads to effective rates of $1/2$ for all I - E pairs, so that we have $\eta_{A,B}^* = \eta_C^*/2 = 1/4$, $x^* = 1/8$, $\lambda_{AA,BB}^* = 1/16$, and $\lambda_{CC}^* = 0$. For $r \rightarrow 1$, the fast ABC dynamics is expected to symmetrize all variables, so that we have $\eta_{A,B,C}^* = 1/3$. Meanwhile, $\lambda_{\alpha\alpha}^* = x^*/2$. To obtain a definite result, we appeal to $3(\lambda_{\alpha\alpha}^* + x^*) = \lambda^* = \eta_A^* + \eta_B^* = 2/3$ and arrive at $x^* = 4/27$ and $\lambda_{\alpha\alpha}^* = 2/27$. Apart from these limiting cases, we can

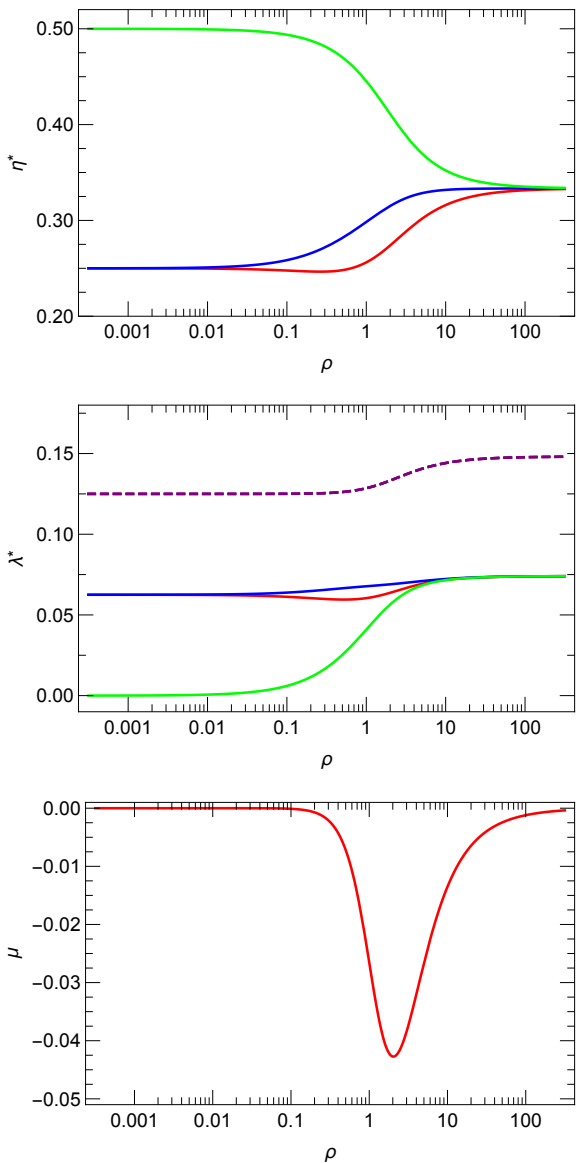


FIG. 3. Solution of the mean-field equation and fixed-point stability analysis, as a function of ρ . Top figure: fixed point values of η , from top to bottom: C (green online), B (blue online), A (red online). Middle figure: fixed point values of λ . Dashed line is for all three types of cross-links. For the self-links, from top to bottom : BB (blue online), AA (red online), CC (green online). Bottom figure: real part of the slowest eigenvalue, μ .

find $(\eta_\alpha^*, \lambda_{\alpha\beta}^*)$ numerically. They are shown, as a function of ρ , in Figs. 3A and B. For finite N , these values differ slightly, for example, by $\sim 1\%$ for $N = 1000$.

Linearizing the evolution equations around the fixed point, we find the following remarkable properties in the spectrum of the stability matrix. There are typically multiple complex conjugate pairs, the real parts of all eigenvalues are negative, so that the fixed point is always *stable*! Except for one complex conjugate pair, the

magnitudes of these real parts are $O(1)$, leading to rapid decay of six modes. Meanwhile, the real part of the last complex conjugate pair, μ , is $O(10^{-2})$ or less, so they are associated with the dominant modes at late times. Plotting μ in Fig. 3C, we find $\mu \rightarrow 0$ at the two limits, indicating that the fixed point becomes marginally stable, as expected. There is also a surprisingly significant dip around $\rho = 2$. At this ρ , the fixed point values are

$$\eta_{A,B,C}^* \cong 0.274, 0.315, 0.411 \quad (10a)$$

$$\lambda_{AA,BB,CC}^* \cong 0.0637, 0.0690, 0.0565 \quad (10b)$$

$$x^* \equiv \lambda_{\alpha \neq \beta}^* \cong 0.133. \quad (10c)$$

The eigenvalues associated with the two slowest modes are $\mu \cong -0.0427 \pm 1.43i$. Meanwhile, the next eigenvalue is -0.853 , so that the next mode decays about 20 times faster. Thus, we can expect the dominant stochastic evolution to take place in a ‘slow plane’ spanned by the eigenvectors of the two slowest modes. The direction of these eigenvectors in phase space encode valuable information. We find the magnitudes of *all* the components are comparable. Thus, all quantities (η, λ) vary with similar amplitudes. The relative phases of the three η components are quite close to $\pm 120^\circ$, reflecting the underlying three-fold cyclic behavior. Meanwhile, the intra-species links $(\lambda_{\alpha\alpha})$ and the cross-links $(\lambda_{\alpha\beta})$ are essentially in phase with η_α and $\eta_\alpha \eta_\beta$, respectively. A significant consequence of the latter is that, even if the amplitudes in η and λ can be large, the ratios $\sigma_{\alpha\beta}$ oscillate with much smaller amplitudes.

The main conclusion of this linear stability analysis is as follows. The trajectory of our system in 8-dimensional space relaxes quickly onto a ‘slow plane.’ In the absence of noise, the phase portrait within this plane is that of a stable spiral such that the dynamics converges to the fixed point $(\eta_\alpha^*, \lambda_{\alpha\beta}^*)$, similar as an underdamped, simple oscillator. Thus, we observe the *stochastic* evolution to be well approximated by noisy oscillations (see Fig. 2). Since fluctuations move the system away from the attractive fixed point, the long time behavior consists of oscillations with random amplitudes (within a finite range, of course). The dominant frequency is given by the imaginary part of the eigenvalue (1.43 here) and comparable to ρ (2 here).

All these properties are consistent with the data from simulations (see Fig. 2), confirming that these mean-field equations capture the typical behavior of the stochastic system. The cross-links, $L_{\alpha\beta}$, oscillate considerably, around the same value with phase lags of $\sim 120^\circ$ (Fig. 2c). The main contributions to these variations are, however, due to the time-dependent, total number of available links: $N_\alpha N_\beta$. When these are factored out, by considering $\sigma_{\alpha\beta}$ instead, we find oscillations which are not only much smaller in amplitudes but also approximately in phase (Fig. 2d). Furthermore, these effective interaction rates, when normalized by $\hat{\sigma} \equiv \sigma / \sum_{\alpha\beta} \sigma_{\alpha\beta}$, are almost constant, varying by at most 5%. These con-

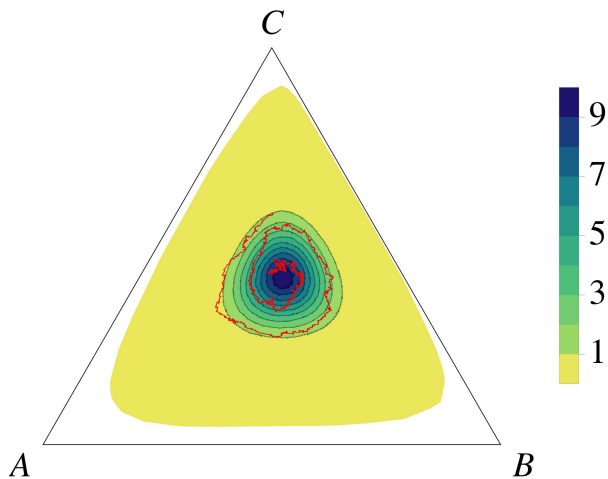


FIG. 4. Contour plot of the frequencies of the occurrence of (A, B, C) during a very long (10^9 MCS) run, representing (a section of) the quasi-stationary distribution, PQSS. The units in the legend are arbitrary; total number of occurrences being the length of the run: 10^9 . Also shown is a typical trajectory (red online) of length 5000 MCS starting near the center at $t=90,022,001$.

stant values

$$\hat{\sigma}_{AB,AC,BC} \cong 0.418, 0.312, 0.270 \quad (11)$$

are entirely consistent with the η_α^* 's [24, 25].

Another perspective of the QSS is the distribution function, $P^{QSS}(\eta_\alpha, \lambda_{\alpha\beta})$, which can be obtained by compiling a histogram with the long time series. Figure 4 shows only the section of P^{QSS} associated with the node variables. Not surprisingly, the central contours are essentially circular, where P^{QSS} is well approximated by a symmetric Gaussian. To illustrate the stochastic nature of the evolution, we also included a short section of the trajectory (red online). This short trajectory begins near the center and spirals away. Later, not shown, it spirals back toward the fixed point.

Unfortunately, while the mathematical analysis shows how the addition of link dynamics and social temperament diversity promotes the coexistence of the species, an intuitively clear picture remains elusive. Here, let us offer a few observations. First, the slight asymmetry in the fixed point values of η_α^* can be argued as follows. Once an A is converted to a C , it starts cutting its links, an in particular those to B . This action implies that it can survive longer than otherwise. Another perspective is that a smaller fraction of C 's participate in the game, leading to a larger total population. Meanwhile, since they 'consume' the A 's and 'feed' the B 's, their abundance can account for the slight difference between A and B . Next, let us focus on the A 's, with the smallest average population. As they near extinction, they are more likely to recover than in the ordinary ABC model, since their predators tend to cut links, thereby reducing those effective interactions. Indeed, in simulations a

strong correlation between $\eta_A \ll 1$ and rapid decrease in the effective rate σ_{CA} is observed, without significant variations in σ_{AB} , the rate they prey on the B 's. A similar, but 'opposite,' scenario appears to be the case for the B 's. As they near extinction, their effective predation rate, σ_{BC} , increases, while their susceptibility to the A 's, σ_{AB} , remain roughly constant. In this sense, the drift towards extinction in the standard ABC model is averted by the action of the introverts.

Finally, we report very similar findings for the $A_E B_I C_I$ case. Changes to equations such as (7) and (23) are minor, only in the $(1-r)$ terms in the $\partial_t \lambda_{B\alpha}$ equations. The most stable system occurs at a slightly different ρ , but is much more stable ($\mu \sim -0.3$). Simulation results are also similar, except that the system are extremely stable, showing few sustained oscillations as fluctuations decay rapidly. Of course, the scenarios painted above must be modified.

IV. SUMMARY AND OUTLOOK

To summarize, in an attempt to merge two standard paradigms in statistical physics, we introduced a simple model to explore co-evolution of node and link degrees of freedom. Specifically, we combined the cyclically competing game of three species with the link dynamics in a population of extreme introverts and extroverts. Whereas the former always ends in extinction within a short time, we find that the addition of link dynamics leads to a surprising long lived state of coexistence when both introverts and extroverts are present. Though a mean field approach, analyzed numerically, provides much insight into this new state, an *intuitive* understanding of how co-evolution and diversity prevent extinction remains elusive.

There are many avenues for further study of this particular model, in addition to the QSS in the complementary $A_E B_I C_I$ case. Interesting issues include incorporating noise into the mean-field equations, analytic perturbative treatments near the two extremes of r , paths of partial population collapse from 6 to 3 node types, possible existence of QSS's involving 4 or 5 types, intrinsically asymmetric interspecies interaction rates, potential emergence of phase transitions between extinction and coexistence, and symmetry in co-evolutionary dynamics near such transitions [44]. Beyond our simple model, many generalizations come to mind readily. One is to impose a structure in the interaction network, such as making it a spatial network [45, 46]. Also, the link dynamics of the original XIE model leads to an extreme Thouless effect [22]. If such a dynamics were implemented, instead of the heatbath dynamics used here, can we expect similar novel phenomena?

Of course, our ABC - XIE model is just a prototype, designed only for a theoretical exploration of the non-equilibrium statistical physics of co-evolution. More realistic complex systems in nature should be considered,

an example being how susceptible individuals would naturally reduce contacts in the presence of an epidemic. In this sense, an SIS model with adaptive networks [47–49] mark the inception of a serious pursuit. Recent work studying competing bacteria colonies that produce and degrade antibiotics are another example [50].

ACKNOWLEDGMENTS

We thank C.I. del Genio, J.J. Dong, T. Gross, J. Knebel, L.B. Shaw, and Z. Toroczkai for illuminating discussions, and especially Güven Demirel during the initial phases of this project. This research is supported in part by the US National Science Foundation, through grant DMR-1507371 (KEB and RKPZ). E.F. acknowledges support by the German Excellence Initiative via the program ‘NanoSystems Initiative Munich’ (NIM).

-
- [1] J. Maynard Smith, *Evolution and the Theory of Games* (Cambridge University Press, 1982).
- [2] E. Frey, *Physica A: Statistical Mechanics and its Applications* **338**, 4265 (2004).
- [3] M. Newman, *SIAM Review* **45**, 167 (2003).
- [4] A.-L. Barabási and M. Psfai, *Network science* (Cambridge University Press, Cambridge, 2016).
- [5] V. Latora, V. Nicosia, and G. Russo, *Complex Networks, Principles, Methods and Applications* (Cambridge University Press, Cambridge, 2017).
- [6] P. Erdos and A. Renyi, *Publicationes Mathematicae* **6**, 290 (1959).
- [7] D. J. de Solla Price, *Science* **149**, 510 (1965).
- [8] A.-L. Barabási and R. Albert, *Science* **286**, 509 (1999).
- [9] M. Paczuski, K. E. Bassler, and A. Corral, *Phys. Rev. Lett.* **84**, 3185 (2000).
- [10] M. Liu and K. E. Bassler, *Phys. Rev. E* **74**, 041910 (2006).
- [11] T. Gross and B. Blasius, *Journal of The Royal Society Interface* **5**, 259 (2008).
- [12] M. Perc and A. Szolnoki, *Biosystems* **99**, 109 (2010).
- [13] H. Sayama, I. Pestov, J. Schmidt, B. J. Bush, C. Wong, J. Yamanoi, and T. Gross, *Computers and Mathematics with Applications* **65**, 1645 (2013).
- [14] J. Hofbauer and K. Sigmund, *Evolutionary games and population dynamics* (Cambridge University Press, Cambridge, UK, 1998).
- [15] A. Dobrinevski and E. Frey, *Phys. Rev. E* **85**, 051903 (2012).
- [16] J. Knebel, T. Krüger, M. F. Weber, and E. Frey, *Physical Review Letters* **110**, 168106 (2013).
- [17] J. Knebel, M. F. Weber, T. Krüger, and E. Frey, *Nature Communications* **6**, 6977 (2015).
- [18] R. K. P. Zia, W. Liu, S. Jolad, and B. Schmittmann, *Physics Procedia* **15**, 102 (2011), proceedings of the 24th Workshop on Computer Simulation Studies in Condensed Matter Physics (CSP2011).
- [19] R. K. P. Zia, W. Liu, and B. Schmittmann, *Physics Procedia* **34**, 124 (2012), proceedings of the 25th Workshop on Computer Simulation Studies in Condensed Matter Physics.
- [20] W. Liu, B. Schmittmann, and R. K. P. Zia, *EPL (Europhysics Letters)* **100**, 66007 (2012).
- [21] W. Liu, B. Schmittmann, and R. K. P. Zia, *Journal of Statistical Mechanics: Theory and Experiment* **2014**, P05021 (2014).
- [22] K. E. Bassler, W. Liu, B. Schmittmann, and R. K. P. Zia, *Phys. Rev. E* **91**, 042102 (2015).
- [23] K. E. Bassler, D. Dhar, and R. K. P. Zia, *Journal of Statistical Mechanics: Theory and Experiment* **2015**, P07013 (2015).
- [24] T. Reichenbach, M. Mobilia, and E. Frey, *Phys. Rev. E* **74**, 051907 (2006).
- [25] M. Berr, T. Reichenbach, M. Schottenloher, and E. Frey, *Phys. Rev. Lett.* **102**, 048102 (2009).
- [26] R. Durrett and S. Levin, *J. Theor. Biol.* **185**, 165 (1997).
- [27] R. Durrett and S. Levin, *Theor. Pop. Biol.* **53**, 30 (1998).
- [28] T. Czárán, *Proc. Natl. Acad. Sci. USA* **99**, 786 (2002).
- [29] B. Kerr, M. Riley, M. Feldman, and B. Bohannan, *Nature* **418**, 171 (2002).
- [30] T. Reichenbach, M. Mobilia, and E. Frey, *Nature* **448**, 1046 (2007).
- [31] T. Reichenbach, M. Mobilia, and E. Frey, *Physical Review Letters* **99**, 238105 (2007).
- [32] T. Reichenbach and E. Frey, *Phys. Rev. Lett.* **101**, 58102 (2008).
- [33] T. Reichenbach, M. Mobilia, A. Zielinski, and E. Frey, *Phys. Rev. E* **87**, 052710 (2013).
- [34] M. F. Weber, G. Poxleitner, E. Heibisch, E. Frey, and M. Opitz, *Journal of The Royal Society Interface* **11**, 20140172 (2014).
- [35] G. Demirel, F. Vazquez, G. Bhme, and T. Gross, *Physica D: Nonlinear Phenomena* **267**, 68 (2014).
- [36] B. Derrida and G. Weisbuch, *EPL (Europhysics Letters)* **4**, 657 (1987).
- [37] M. N. Barber and B. Derrida, *Journal of Statistical Physics* **51**, 877 (1988).
- [38] A. Coniglio, L. de Arcangelis, H. J. Herrmann, and N. Jan, *EPL (Europhysics Letters)* **8**, 315 (1989).
- [39] D. T. Gillespie, *Journal of Computational Physics* **22**, 403 (1976).
- [40] A. Szolnoki, M. Mobilia, L.-L. Jiang, B. Szczesny, A. M. Rucklidge, and M. Perc, *Journal of The Royal Society Interface* **11**, 20140735 (2014).
- [41] N. Masuda and N. Konno, *Physical Review E* **74**, 066102 (2006).
- [42] G. Szabó and G. Sznaider, *Phys. Rev. E* **69**, 2 (2004).
- [43] Note that $\rho \in [0, (N - 1) / 2]$ and approaches $[0, \infty]$ in the thermodynamic limit. For simplicity, we keep ρ finite in our numerical analysis and so, we have $1 - r = 1 - 2\rho/N \rightarrow 1$ below.
- [44] S. Hossein, M. D. Reichl, and K. E. Bassler, *Phys. Rev. E* **89**, 042808 (2014).
- [45] M. Penrose, *Random Geometric Graphs* (Oxford University Press, Oxford, 2003).
- [46] A. Nyberg, T. Gross, and K. E. Bassler, *Journal of Complex Networks* **3**, 543 (2015).
- [47] T. Gross, C. J. D. D’Lima, and B. Blasius, *Phys. Rev. Lett.* **96**, 208701 (2006).
- [48] L. B. Shaw and I. B. Schwartz, *Phys. Rev. E* **77**, 066101 (2008).
- [49] S. Jolad, W. Liu, B. Schmittmann, and R. K. P. Zia, *PLoS ONE* **7**, 1 (2012).
- [50] E. D. Kelsic, J. Zhao, K. Vetsigian, and R. Kishony, *Nature* **521**, 516 (2015).

V. APPENDIX

Here, we provide some details of the equations for the evolution of $L_{\alpha\beta}$. The terms stemming from link updates, being proportional to $(1-r)$, are easily understandable. Those needed to account for a node update are more involved; see thick arrows in Fig. 1. In the main

text, we discussed how the leading terms associated with the probability of 3-node clusters arise. However, there is no unique scheme for the next leading terms. Here, we choose a set which reduces properly to the original ABC model (a fully connected population) in the limit of $r = 1$. The result is

$$\partial_t L_{AA} = r \left\{ \frac{L_{AB}L_{AB}}{N_B} - 2\frac{L_{AA}L_{AC}}{N_A} - \frac{L_{AC} + L_{AB}}{2} \right\} - (1-r) \left\{ L_{AA} - \frac{N_A(N_A-1)}{2} \right\} \quad (12)$$

$$\partial_t L_{BB} = r \left\{ \frac{L_{BC}L_{BC}}{N_C} - 2\frac{L_{BB}L_{BA}}{N_B} - \frac{L_{BC} + L_{BA}}{2} \right\} - (1-r) \left\{ L_{BB} - \frac{N_B(N_B-1)}{2} \right\} \quad (13)$$

$$\partial_t L_{CC} = r \left\{ \frac{L_{CA}L_{CA}}{N_A} - 2\frac{L_{CC}L_{CB}}{N_C} - \frac{L_{CB} + L_{CA}}{2} \right\} - (1-r) \{L_{CC}\} \quad (14)$$

$$\partial_t L_{AB} = r \left\{ \frac{L_{BC}L_{CA}}{N_C} - \frac{L_{AB}L_{AC}}{N_A} + 2\frac{L_{BB}L_{BA}}{N_B} - \frac{L_{AB}L_{AB}}{N_B} + L_{AB} \right\} - (1-r) \{L_{AB} - N_A N_B\} \quad (15)$$

$$\partial_t L_{CA} = r \left\{ \frac{L_{CB}L_{BA}}{N_B} - \frac{L_{CA}L_{CB}}{N_C} + 2\frac{L_{AA}L_{AC}}{N_A} - \frac{L_{CA}L_{AC}}{N_A} + L_{CA} \right\} - (1-r) \left\{ L_{CA} - \frac{N_C N_A}{2} \right\} \quad (16)$$

$$\partial_t L_{BC} = r \left\{ \frac{L_{CA}L_{AB}}{N_A} - \frac{L_{CB}L_{BA}}{N_B} + 2\frac{L_{CC}L_{CB}}{N_C} - \frac{L_{CB}L_{CB}}{N_C} + L_{CB} \right\} - (1-r) \left\{ L_{CB} - \frac{N_C N_B}{2} \right\} \quad (17)$$

It is straightforward to verify that setting r to unity and substituting $L_{\alpha\alpha} = N_\alpha(N_\alpha - 1)/2$ and $L_{\alpha\beta} = N_\alpha N_{\beta \neq \alpha}$ into Eqns. (12-17) gives us the same set as Eqns. (2).

Keeping these next-to-leading order terms, the total number of links, $\mathcal{L} \equiv \pm_\alpha L_{\alpha\alpha} + \pm_{\alpha \neq \beta} L_{\alpha\beta}$, satisfies the simple equation

$$\partial_t \mathcal{L} = (1-r) \{(N-1)(N-N_C)/2 - \mathcal{L}\} \quad (18)$$

As for fixed points, the following results are trivial: $L_{AB}^* = L_{BC}^* = L_{CA}^* \equiv X^*$, $\mathcal{L}^* = (N-1)(N-N_C^*)/2$. Thus, the number of independent variables reduces to

five. Nevertheless, the analytic forms of $(N_\alpha^*, L_{\alpha\beta}^*)$ are, in general, quite complex. The exception are, as in the main text, the $r \rightarrow 0, 1$ limits. Here, we provide the next-to-leading terms as well. For the former ($r \rightarrow 0$), we have $N_{A,B}^* = N_C^*/2 = N/4$, $X^* = N^2/16$, $L_{AA,BB}^* = N(N-4)/32$, and $L_{CC}^* = 0$. For $r \rightarrow 1$, the fast ABC dynamics is expected to symmetrize all variables, so that we have $N_{A,B,C}^* = N/3$. Exploiting $\mathcal{L}^* = (N-1)(N-N_C^*)/2$, the final results are $X^* = 2N(N+1)/27$ and $L_{\alpha\alpha}^* = N(N-7/2)/27$.

Finally, let us present the full set of equations for the fractions, in the thermodynamic limit:

$$\partial_t \eta_A = \rho(\lambda_{AB} - \lambda_{CA}); \quad \partial_t \eta_B = \rho(\lambda_{BC} - \lambda_{AB}); \quad \partial_t \eta_C = \rho(\lambda_{AC} - \lambda_{BC}) \quad (19)$$

$$\partial_t \lambda_{AA} = \rho \left\{ \frac{\lambda_{AB}^2}{\eta_B} - 2\frac{\lambda_{AA}\lambda_{AC}}{\eta_A} \right\} - \{\lambda_{AA} - \eta_A^2\} \quad (20)$$

$$\partial_t \lambda_{BB} = \rho \left\{ \frac{\lambda_{BC}^2}{\eta_C} - 2\frac{\lambda_{BB}\lambda_{BA}}{\eta_B} \right\} - \{\lambda_{BB} - \eta_B^2\} \quad (21)$$

$$\partial_t \lambda_{CC} = \rho \left\{ \frac{\lambda_{CA}^2}{\eta_A} - 2 \frac{\lambda_{CC} \lambda_{CB}}{\eta_C} \right\} - \lambda_{CC} \quad (22)$$

$$\partial_t \lambda_{AB} = \rho \left\{ \frac{\lambda_{BC} \lambda_{CA}}{\eta_C} - \frac{\lambda_{AB} \lambda_{AC}}{\eta_A} + 2 \frac{\lambda_{BB} \lambda_{BA}}{\eta_B} - \frac{\lambda_{AB}^2}{\eta_B} \right\} - \{\lambda_{AB} - 2\eta_A \eta_B\} \quad (23)$$

$$\partial_t \lambda_{CA} = \rho \left\{ \frac{\lambda_{CB} \lambda_{BA}}{\eta_B} - \frac{\lambda_{CA} \lambda_{CB}}{\eta_C} + 2 \frac{\lambda_{AA} \lambda_{AC}}{\eta_A} - \frac{\lambda_{CA}^2}{\eta_A} \right\} - \{\lambda_{CA} - \eta_C \eta_A\} \quad (24)$$

$$\partial_t \lambda_{CB} = \rho \left\{ \frac{\lambda_{CA} \lambda_{AB}}{\eta_A} - \frac{\lambda_{CB} \lambda_{BA}}{\eta_B} + 2 \frac{\lambda_{CC} \lambda_{CB}}{\eta_C} - \frac{\lambda_{CB}^2}{\eta_C} \right\} - \{\lambda_{CB} - \eta_C \eta_B\} \quad (25)$$

where, of course, η_C stands for $1 - \eta_A - \eta_B$. We should emphasize that, in this limit, the period of typical oscil-

lations is of the order of $1/\rho$, since they are controlled by the ABC dynamics.